Cleaner Engineering and Technology 31 (2026) 101178

Contents lists available at ScienceDirect

Cleaner Engineering and Technology

journal homepage: www.sciencedirect.com/journal/cleaner-engineering-and-technology

Optimized one-pot room-temperature interfibrillar synthesis of silver nanoparticles using cotton fiber as reductant for pathogen-resistant protective textiles

Md Nayeem Hasan Kashem [a,b], Sunghyun Nam [a,*], Matthew B. Hillyer [a], Faqrul Hassan [a,b], Sanjay Joshi [b,c], Tia Zimmerman [c], Gillian Bruni [c], Holly King [d], Doug Hinchliffe [a,d], David Fang [a]

[a] Cotton Fiber Bioscience and Utilization, Southern Regional Research Center, U.S. Department of Agriculture, Agricultural Research Service, New Orleans, LA, 70124, USA
[b] Oak Ridge Institute for Science and Education, United States Department of Energy, 1299 Bethel Valley Road, Oak Ridge, TN, 37831-0117, USA
[c] Commodity Utilization Research, Southern Regional Research Center, U.S. Department of Agriculture, Agricultural Research Service, New Orleans, LA, 70124, USA
[d] Cotton Quality and Innovation, Southern Regional Research Center, U.S. Department of Agriculture, Agricultural Research Service, New Orleans, LA, 70124, USA

ARTICLE INFO

Keywords:
Nanotechnology
Silver nanoparticles
Cotton fiber
Antibacterial fabric

ABSTRACT

Silver nanoparticles (AgNPs) incorporated cotton fabrics offer broad applications; however, conventional syntheses rely on toxic and costly reducing agents, involve complex multi-step and energy-intensive processing, and result in poor laundering performance due to surface-bound nanoparticle deposition. Herein, a simplified one-pot, room-temperature method is reported to produce AgNP-incorporated cotton (NanoAgCot), with cotton fiber acting as the sole reducing agent under alkaline conditions. This simple process yields highly uniform nanoparticles (14.74 ± 6.61 nm in diameter) distributed on both the fiber surface and interfibrils, achieving a high loading of 22,888 ± 2967 mg kg^{-1} without an external reducing agent, stabilizing agent, heat, or light. Nanoparticle growth conditions were optimized using Sequential Least Squares Quadratic Programming (SLSQP), varying alkali concentration and reaction time. The NanoAgCot fabric exhibited excellent wash durability, retaining over 55 % of nanoparticles after 50 machine-wash cycles. Importantly, the fabric displayed potent antibacterial properties, achieving complete inhibition of the plant pathogen *Pantoea agglomerans,* evaluated for the first time in the context of AgNP-incorporated cotton fabric, as well as *Bacillus subtilis*, and 99.997% and >99.9997% inhibition of the clinical pathogens *Pseudomonas aeruginosa* and *Staphylococcus aureus*, respectively. These findings highlight the potential of this approach to deliver cost-effective, material-saving, and wash-durable antimicrobial cotton fabrics, suitable for protective clothing for agricultural workers and healthcare professionals in high-risk environments.

1. Introduction

Cotton is a widely used natural cellulose fiber in casual clothing, sportswear, medical textiles, and hygiene products due to its inherent properties, such as softness, breathability, sweat absorption, and comfort (Chen and Chiang, 2008; Vance et al., 2015). However, the hygroscopic nature of cotton makes it highly susceptible to microbial growth, limiting its long-term functionality and hygiene (Chen and Chiang, 2008; Islam et al., 2021; Lim and Hudson, 2004). To address this challenge, extensive efforts have been directed toward modifying cotton fibers to develop next-generation smart textiles with antimicrobial and multifunctional properties.

In recent years, nanoengineering has emerged as a versatile strategy for imparting advanced functionalities into cotton fabrics. The immobilization of nanoparticles on cotton fabric incorporates diverse properties, such as antibacterial activity (Nam et al., 2020; Nam et al., 2021), hydrophobicity (Kashem et al., 2025; Seth and Jana, 2022), catalytic behavior (Hillyer et al., 2024; Kumar et al., 2020; Qi et al., 2020), oil-water separation capabilities (Cao et al., 2023; Meresht et al., 2025), energy harvesting (Dolez, 2021; Xiong et al., 2017), and wearable biosensors (Fu et al., 2024; Shi et al., 2023). Among the various nanomaterials explored, silver nanoparticles (AgNPs) have garnered

* Corresponding author. Cotton Fiber Bioscience and Utilization, Southern Regional Research Center, U.S. Department of Agriculture, Agricultural Research Service, New Orleans, LA, 70124, USA.
E-mail addresses: Mdnayeem.Kashem@usda.gov (M.N.H. Kashem), sunghyun.nam@usda.gov (S. Nam).

https://doi.org/10.1016/j.clet.2026.101178
Received 29 December 2025; Received in revised form 14 February 2026; Accepted 28 February 2026
Available online 2 March 2026

particular attention due to the broad applications in catalysis, optics, electronics, water purification, and antimicrobial consumer products (Ali et al., 2017; Chou et al., 2005; Tang et al., 2012; Yazdanshenas and Shateri-Khalilabad, 2013). Several methods have been developed to incorporate AgNPs into textiles, including dip coating (Balamurugan et al., 2017), colloidal surface coating (Lee et al., 2003), *in situ* reduction (Nam and Condon, 2014), and layer-by-layer (Dubas et al., 2006). Most conventional AgNP syntheses rely on chemical reducing agents, for example, ascorbic acid, hydrazine, *N*,*N*-dimethylformamide or sodium borohydride to control particle nucleation, size, and shape while preventing agglomeration (Nam et al., 2024; Pranto et al., 2025). For textile applications, many studies reported using natural plant extracts, i.e., leaf extracts of E. globulus and C. alata, as reducing agents for AgNP extraction during green synthesis (Salgado et al., 2023; Sivaranjana et al., 2017). On the other hand, cellulose itself can act as a reducing agent under mild alkaline hydrothermal conditions for the synthesis of various metal oxides (Emam and El-Bisi, 2014; Guodong et al., 2012; Li et al., 2012; Yazdanshenas and Shateri-Khalilabad, 2012). However, all these processes involve multiple steps, uncontrolled nanoparticle growth resulting in agglomeration, insufficient nanoparticle deposition, and the need for elevated temperatures, therefore, posing higher costs and manufacturing challenges for sustainable textile production (El-Seedi et al., 2019; Yazdanshenas and Shateri-Khalilabad, 2013). More critically, most prior studies report nanoparticle formation primarily on the fiber surface, leading to poor washing durability and limited practical applicability (see Table S1 for a detailed analysis of the shortcomings of different synthesis approaches). Therefore, developing a simple, low-cost, energy-saving, and controllable *in situ* synthesis strategy for wash-durable AgNP cotton fabric remains a pressing issue for commercial textile production and research community for developing multifunctional fabric.

The development of antimicrobial fabrics is especially critical for reducing health risks posed by pathogenic bacteria in agricultural and clinical environments. *Pantoea agglomerans*, a gram-negative bacterium commonly found in plants (e.g., beans, sugarcane), soils, and feculent materials, has emerged as an opportunistic pathogen associated with nosocomial infections, neonatal sepsis, and bacteremia (Andersson et al., 1999; Cruz et al., 2007; Li et al., 2024; Mani and Nair, 2021; Mardaneh and Pouresmaeil, 2024; Sengupta et al., 2016). Beyond human health, it also causes plant diseases, highlighting its dual significance in agriculture and medicine (Dutkiewicz et al., 2016; Zhang et al., 2025). However, the antimicrobial efficacy of AgNP incorporated fabric against *Pseudomonas aeruginosa* has not yet been explored in literature to the best of our knowledge. Although *Bacillus subtilis* (gram-positive) is generally regarded as a nonpathogenic plant-based bacterium, it can cause secondary infections in immunocompromised patients, including dermal wounds, burns, and respiratory or urinary tract infections, which may become life-threatening (Nicolas et al., 2012; Saleh et al., 2014). Transmission of these bacteria can occur through thorn or splinter injuries in farm settings, inhalation of contaminated dust, or exposure to contaminated medical fluids (Dutkiewicz et al., 2016; Mirtella et al., 2021). Similarly, *Staphylococcus aureus* (gram-positive) and *Pseudomonas aeruginosa* (gram-negative) are among the most widespread human pathogens, responsible for hospital- and community-acquired infections, as well as chronic wound complications (Ekunde et al., 2025; Fazli et al., 2009; Trizna et al., 2020). Given that these pathogens can originate from both plant-based sources and hospital environments, there is a critical need for antimicrobial clothing that is breathable, wash-resistant, and comfortable, made from natural cotton produced via a streamlined, resource-efficient fabrication method, to safeguard agricultural workers from plant-associated bacteria and healthcare professionals from hospital-acquired infections.

Herein, a one-pot, room-temperature strategy is reported for the *in situ* synthesis of silver nanoparticles (AgNPs) within cotton fibers. A homogeneous distribution of nanoparticles is expected within the fiber interior and on the fiber surface at room temperature, without the need for an external reducing agent, stabilizing agent, external heat, or light. The bean-shaped multilayer cotton fiber structure temporarily swells and opens microchannels for the diffusion of precursor silver ions inside the lumen under alkaline conditions (Nam and Condon, 2014). The abundance of hydroxyl groups in the activated cellulose thereby transforms these micro-channels into micro-bioreactors and should be sufficient for the reduction of Ag^+ at room temperature without additional chemical agents. The hypothesis can further be validated through a systematic study of the effects of reaction time and alkali concentration on nanoparticle growth and homogeneous distribution throughout the cotton fiber. To demonstrate the advantages of distributing AgNPs within the fiber matrix rather than depositing them only on the fiber surface, laundering durability was investigated. The antibacterial properties of AgNP-incorporated cotton fabrics were investigated against plant-based and typical hospital-associated pathogens. For comparison, the advantages of this proposed synthesis approach are tabulated alongside the existing literature in Table S1. Overall, the study addresses a critical need for low-cost, scalable, and durable antimicrobial cotton materials, with potential applications across agricultural, industrial, and healthcare sectors.

2. Experimental section

2.1. Materials

Commercial cotton fabric (scoured and bleached, areal density: 94.50 ± 2.70 g/m^2, thickness: 243.20 ± 9.20 μm) was procured from Testfabrics, Inc., and used without any modification (Style 400, West Pittston, PA, USA). Commercial cotton fibers typically consist of 88–96% cellulose, 1.1–1.9% protein, 0.7–1.2% pectic substances, 0.7–1.6% waxes, 0.4–1.0% sugars, 0.5–1.0% organic acids, and other minor constituents (Wakelyn et al., 2006). Following scouring and bleaching, the cellulose content increases to ≥99%, with a degree of polymerization in the range of 9000–15,000 (Cotton Inc). Sodium hydroxide (NaOH) at 50% w/v and nitric acid (HNO3) at 68-70% w/w were purchased from Sigma-Aldrich. Silver nitrate ($AgNO_3$, 99.9%) was purchased by J. T. Baker (Phillipsburg, NJ, USA). All the chemicals were utilized as received. Ultra-pure water with a resistance of 18.0 MΩ/cm was used in the experiments.

2.2. Fabrication of NanoAgCot fabric

Fig. 1a depicts the fabrication technique. Briefly, 0.1 g of silver nitrate ($AgNO_3$) was added to 100 mL of deionized (DI) water to prepare a 0.1% (w/v) precursor solution. The solution was stirred for 5 min to ensure complete dissolution. A 50 mL aliquot of this solution was used to soak a piece of white cotton fabric (0.5 g; 2 in. × 4 in.) for 1 h, with pH adjusted using dilute HCl or NaOH as necessary. This step promotes rapid sorption of Ag^+ inside the cellulose network. Subsequently, NaOH solutions of varying concentrations (0.05%, 0.14%, 0.24%, 0.48%, 0.94%, 1.39%, and 2.29% w/v) were added to the reaction mixture and vortexed for 8 h for ensuring homogeneous reaction conditions. NaOH concentration was calculated as mass of NaOH per total volume of the reaction mixture. Upon completion of the reaction, the fabric turned brown or dark brown, depending on the extent of nanoparticle content in the cotton fibers. Next, DI water and AATCC standard detergent (0.37% w/v) were applied to the fabric for 30 min at ambient temperature for washing, stirred in a flask with a large stir bar to remove loosely attached nanoparticle lump. After drying under ambient conditions, the sample was further washed with DI water at 70 °C for 2 h to remove any residual precursor ions or unbound nanoparticles. Finally, the fabric was dried in ambient conditions.

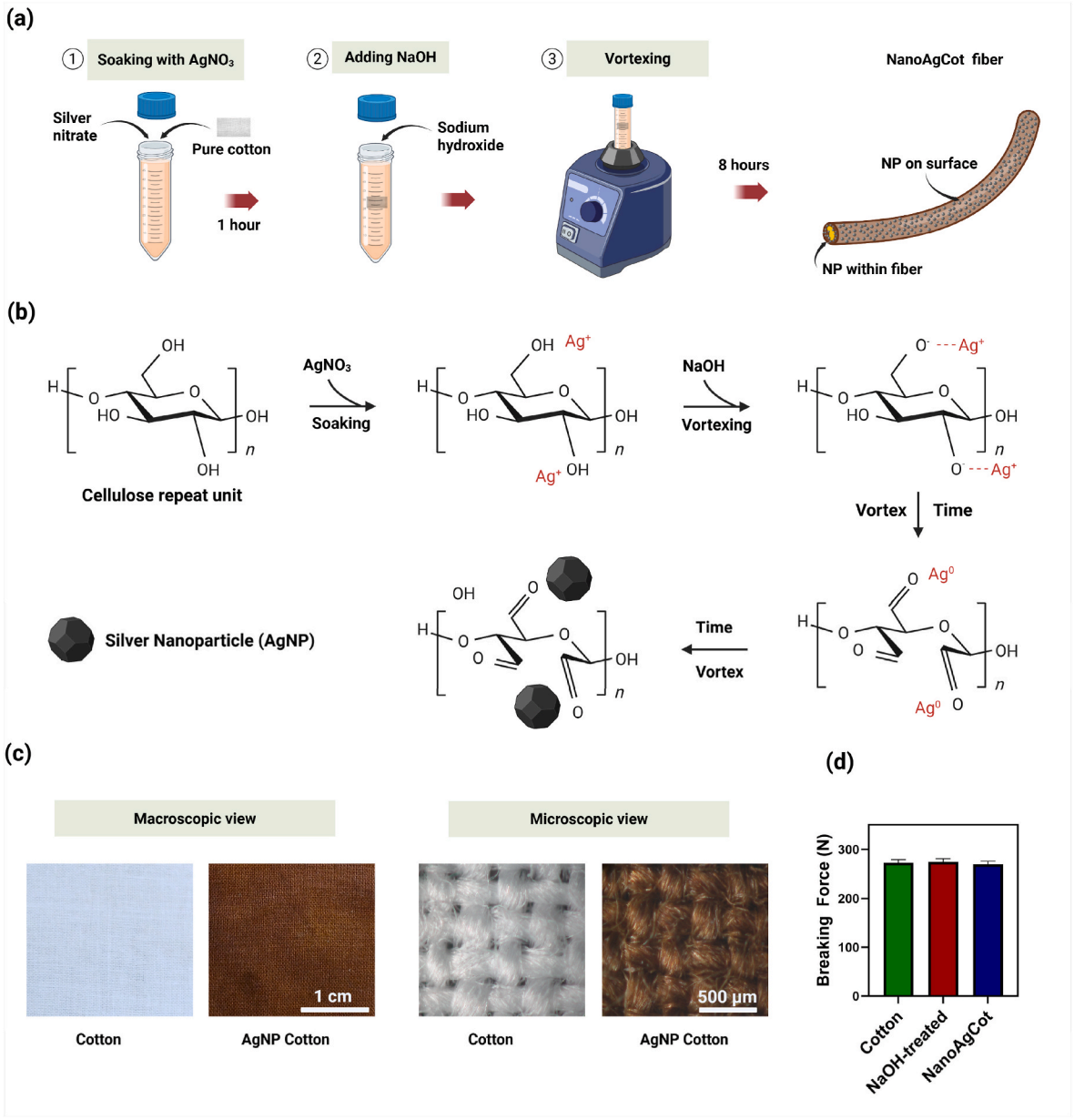

Fig. 1. Room-temperature, one-pot synthesis of interfibrillar AgNPs on cotton. (a) Process schematic: (1) $AgNO_3$ soaking loads Ag^+ throughout the fiber; (2) NaOH deprotonates cotton fiber and temporarily swells (molecularly or nanoscopically) cotton and facilitates deep diffusion of Ag^+ ions; (3) vortexing maintains mass transfer during cellulose-mediated reduction to Ag^0. (b) Proposed pathway: Ag^+ coordination to cellulose → Ag-O coordination bond formation in the presence of NaOH → electron transfer from alkaline cellulose to Ag^0 → growth of immobilized AgNPs within the surface and interfibrillar matrix. (c) Macroscopic and microscopic images of pristine cotton and NanoAgCot fabrics; (d) Strip test analysis of pristine cotton, NaOH-treated cotton and NanoAgCot fabrics in the warp direction.

2.3. Characterization of cotton

2.3.1. UV-vis spectroscopy

Reflection ultraviolet-visible (UV–vis) spectroscopical analysis was performed using an ISR-2600 spectrometer (Shimadzu, Japan) over the 200–900 nm range, with a spectral resolution of 1 nm.

2.3.2. Optical imaging

Optical images of different fabrics were acquired using a digital microscope (KH-8700, Hirox). The colorimetric values (a, b, x, and y) were calculated using Python image processing. The total color difference was calculated using the following formula:

$$\Delta E = \sqrt{(L - L_0)^2 + (a - a_0)^2 + (b - b_0)^2} \quad \text{Eq. (1)}$$

Here, L_0 , a_0, and b_0 are the reference values of L, a and b. The average values of three trials are presented.

2.3.3. Scanning electron microscopy (SEM)

Scanning electron microscopy (SEM) and elemental mapping of silver (Ag) were performed on various samples using a Phenom G6 ProX (Nanoscience Instruments, Phoenix, AZ, USA). At first, a carbon tape (double-sided) was used to mount the sample on a sample stub. A gold coating with 7 nm thickness was sputter-coated using a sputter coater (LUXOR, Aptco Technologies, Belgium). For image collection, accelerating voltages at 10 kV and 15 kV were used, with magnifications of 2000 × , 1500 × , and 1000 × . Samples for cross-sectional analysis were prepared according to the protocols described in section 2.3.5 and placed on a carbon tape (double-sided) for imaging.

2.3.4. X-ray diffractometry (XRD)

The fabrics were characterized by X-ray diffractometry (XRD) analysis utilizing Rigaku Miniflex (Rigaku Americas Corporation, The Woodlands, TX, USA) with (5° - 80°) angular scanning (2θ), 0.1° step size, and 5°/min scan rate.

2.3.5. Transmission electron microscopy (TEM)

The cross-section of cotton fiber samples was illustrated by Transmission electron microscope (TEM) (FEI Tecnai G2 F30). Samples for TEM were prepared following published methods (Boylston et al., 1991; Thibodeaux and Evans, 1986) Briefly, the samples were embedded in a resin system composed of butyl methacrylate, methyl methacrylate, and benzoyl peroxide, and polymerized using a UV cross-linking unit (CL-1000, Analytik, Germany). Ultrathin sections with a thickness of approximately 100 nm were then obtained using a microtome (PowerTome Ultramicrotome, Boeckeler Instruments, USA). The resulting sections were mounted on copper grids (carbon-coated) and subsequently imaged by TEM with an operating voltage of 300 kV.

2.3.6. Atomic absorption microscopy (AAS)

An atomic absorption spectrometer (240Z AA with graphite furnace, Agilent, USA) was used to detect silver content in the cotton fibers. At first, 0.02 g of cotton fabric was weighed. Then, utilizing a microwave digestion system, the sample was digested in nitric acid (10 mL, 6 M) (MARS 6, CEM Corporation, USA). The digested solution was collected and diluted to 1:1000 (w/w). Next, the solution was analyzed using a calibration curve, which was established by a silver (Ag) standard solution (Agilent, Santa Clara, CA, USA). The final measurement was determined from the average of three samples.

2.3.7. X-ray photoelectron spectrometer (XPS)

X-ray photoelectron spectroscopy (XPS) analyses were performed using a Physical Electronics PHI 5000 VersaProbe II Hybrid spectrometer operated under ultra-high vacuum conditions, with the analysis chamber pressure maintained below 1×10^{-7} Pa. A monochromated Al Kα X-ray source ($h\nu = 1486.6$ eV) was employed at an operating power of 25 W and an accelerating voltage of 15 kV, using an analysis spot size of 100 μm. Wide-scan (survey) spectra were acquired over a binding energy range of 0–1400 eV with a pass energy of 187.85 eV and an energy step size of 0.8 eV. To obtain a high-resolution spectrum, a reduced pass energy of 23.5 eV and a step size of 0.1 eV were set. The binding energy calibration was calculated by referencing all spectra to the adventitious carbon C 1s peak at 284.6 eV.

2.3.8. Tensile strength test

Tensile strength measurements for pristine and NanoAgCot fabrics were conducted in accordance with ASTM D5035-95, utilizing a universal testing machine (Instron 5566, USA). For each fabric type, five specimens measuring 1.5 × 6 inches were prepared and tested along the warp direction.

2.4. Laundering test

Laundering durability was evaluated according to AATCC Test Method 61-2007 using a laboratory laundry machine, the Launder-Ometer (M228-AA, SDL Atlas, LLC, USA). At first, 200 mL of 0.37% (w/v) AATCC standard detergent solution and ten stainless-steel balls were added to a stainless-steel canister to simulate mechanical agitation. The canister was preheated to 40.0 ± 0.1 °C. A NanoAgCot Swatch (2 in. × 4 in.) was introduced to the canister. Washing was conducted at a fixed temperature of 40.0 ± 0.1 °C and a rotational speed of 40 ± 2 rpm for 45 min. Each cycle corresponded to five conventional home or commercial laundering washes, with fabrics subjected to 10 cycles, equivalent to 50 conventional washes. Following laundering, samples were rinsed with deionized water at room temperature for 10 min to remove residual detergent and air-dried under ambient conditions. The remaining silver was quantified using Atomic Absorption Spectroscopy (GFAAS) and UV–vis spectroscopy. Silver retention was calculated using the formula:

$$\%[Ag] = \frac{I_0 - I_n}{I_0} \times 100 \quad \text{Eq. (2)}$$

Here, I_0 and I_n represent the silver concentration at cycle 0 and cycle n, respectively, as determined by GFAAS or UV–vis analysis.

2.5. Antimicrobial test

The antibacterial activity of the nanoparticle-embedded fabrics was assessed following the AATCC 100:2012 antimicrobial fabric test standard. Briefly, circular samples (1.9-inch diameter) of both pristine cotton and NanoAgCot fabrics were sterilized by autoclaving. Bacterial strains *Pantoea agglomerans* BSDF19-4 and *Bacillus subtilis* BSDF49-1 (Qi et al., 2025) were grown as precultures either in MRS (Research Products International, Mount Prospect, IL, USA ("de man, rogosa and sharpe (MRS) agar," 2003)) or Tryptone Sucrose Yeast (TSY) medium with 50 g/L sucrose, adapted from (Haynes et al., 1955) and normalized to 10^5 colony-forming units/mL. Inoculum was plated to confirm CFU/mL. The fabric samples were treated by soaking each in 1 mL of the inoculum containing approximately 10^5 colony-forming units (CFU) of the bacterial isolate for 1 min allowing the solution to be fully absorbed by the fabric. After inoculation, the treated fabric samples were transferred to individual sterile glass jars for zero-time and 24-h incubation. Next, 100 mL of sterile 1X PBS was added to the zero-time incubation group immediately after placing the bacteria-inoculated swatches in the jar. After vigorous shaking, serial dilutions of 10^0, 10^{-1}, and 10^{-2} were prepared. Then, 100 μL of each dilution was spread in triplicate onto MRS or Nutrient agar plates (Research Products International, Mount Prospect, IL, USA) using an Eddy Jet 2W Automatic Spiral Plater in linear 100 mode (Neutec Group, Inc., NY, USA). The inoculated plates were incubated overnight at 28 °C. Colonies were counted with the SphereFlash Automatic Colony Counter (Neutec Group, Inc., NY, USA) using the SphereFlash Colonies PRO software version 1.0.0.16, and results were expressed as CFU/mL. Additionally, for the 24-h time point, the jars were incubated for 24 h at 28 °C, and then the same serial dilution procedure was performed as for the time-zero group.

Antibacterial performance against *Staphylococcus aureus* (ATCC 6538) and *Pseudomonas aeruginosa* (ATCC 9027) was evaluated at Microchem Laboratory (Texas, USA) in accordance with the AATCC Test Method 100-2004, titled *"Antibacterial Finishes on Textile Materials: Assessment of Antibacterial Activity."* The antibacterial efficacy was quantified by calculating the percentage reduction in bacterial growth using the following equation:

$$\%\ inhibition = \left(\frac{B - A}{B}\right) \times 100 \quad \text{Eq. (3)}$$

where A denotes the number of test bacteria recovered from the NanoAgCot sample after 24 h of contact, and B represents the number of test bacteria on the control sample (pristine cotton) immediately following inoculation.

3. Results

3.1. Fabrication process of NanoAgCot fabric

Fig. 1 illustrates the one-pot, room-temperature synthesis technique of silver nanoparticles distributed both within the internal matrix and on the surface of fibers. As shown in Fig. 1a, pristine cotton fabric was first immersed in $AgNO_3$, which promotes rapid sorption of Ag^+ inside the cellulose network (β (1–4) linked D-glucose chain network). Upon the addition of NaOH and vortexing, two simultaneous processes drive *in situ* silver nanoparticle formation as shown in Fig. 1b. First, alkalization

deprotonates cotton fiber because of its relatively low pK_a (<10.2) (Heymann & Rabinov, 1941; Österberg and Claesson, 2000), which creates more reaction sites. The Ag^+ binds readily to polysaccharide oxygen donors and provides a dense distribution of cation adsorption sites on and within cellulosic substrates (Salama et al., 2021). Importantly, the alkaline treatment swells the cotton fiber from bean shape to round shape, providing micro-channels inside the layered structure (Nam and Condon, 2014). Therefore, the alkaline treatment, coupled with vortexing, increases diffusion pathways, thereby transporting Ag^+ deeper into interfibrillar domains where it can nucleate *in situ*. Second, the reduction proceeds without an added reducing agent because cellulose acts as an electron donor under alkaline conditions that produces Ag^0 ($Ag^+ \rightarrow Ag^0$) and converts hydroxyl groups to carbonyls (Fig. 1b) (Emam and Ahmed, 2016; Guodong et al., 2012; Tsague et al., 2024). With time, the size of the nanoparticle increases. In contrast to conventional approaches to cotton, which often require additional chemistries such as ammonia/Tollens' reagent, plasma activation, or pre-oxidized cellulose substrates, this ambient, two-reagent protocol offers an atom-economic alternative.

Macroscopically, the white cotton fabric transitions to a brown/dark brown hue following complete nanoparticle synthesis (Fig. 1c), consistent with metallic AgNPs as reported before (Nam and Condon, 2014; Yazdanshenas and Shateri-Khalilabad, 2013). Optical microscopic images confirmed that the treatment preserved the fabric's structural integrity on a microscopic scale. Additionally, strip tensile testing (Fig. 1d) performed along the warp direction revealed no statistically significant difference in breaking force between pristine cotton (272 ± 6 N) and NanoAgCot fabrics (270 ± 5 N), synthesized using 1.39 wt% NaOH for 8 h at pH 5.3 (as described later in the manuscript). To isolate the effect of alkaline treatment, cotton fabric was treated with 1.39 wt% NaOH under identical reaction conditions in the absence of $AgNO_3$. The NaOH-treated cotton exhibited a comparable breaking force (274 ± 5 N) to that of pristine cotton, confirming that the mild alkaline treatment did not induce measurable cellulose degradation or compromise mechanical integrity. Similarly, no statistically significant change in breaking force was observed in the weft direction in pristine cotton and NanoAgCot fabrics, as shown in Fig. S1a. On the other hand, elongation at break measured in the warp direction (Fig. S1b) increased slightly for both NaOH-treated cotton (8.60% ± 0.21%) and NanoAgCot (8.93% ± 0.14%) compared to pristine cotton (6.61% ± 0.13%). This modest increase may be attributed to structural relaxation or slight shrinkage, occurring during the washing and drying steps rather than cellulose degradation. Therefore, these findings confirm that the synthesis process preserves the mechanical integrity of the cotton substrate. Fig. S2 indicates the thickness and areal density of fabrics before and after nanoparticle synthesis. Both thickness and areal density slightly increase after nanoparticle synthesis. These findings suggest that NanoAgCot fabric retains the texture and durability of untreated fabric, supporting its potential for substitution in numerous textile applications.

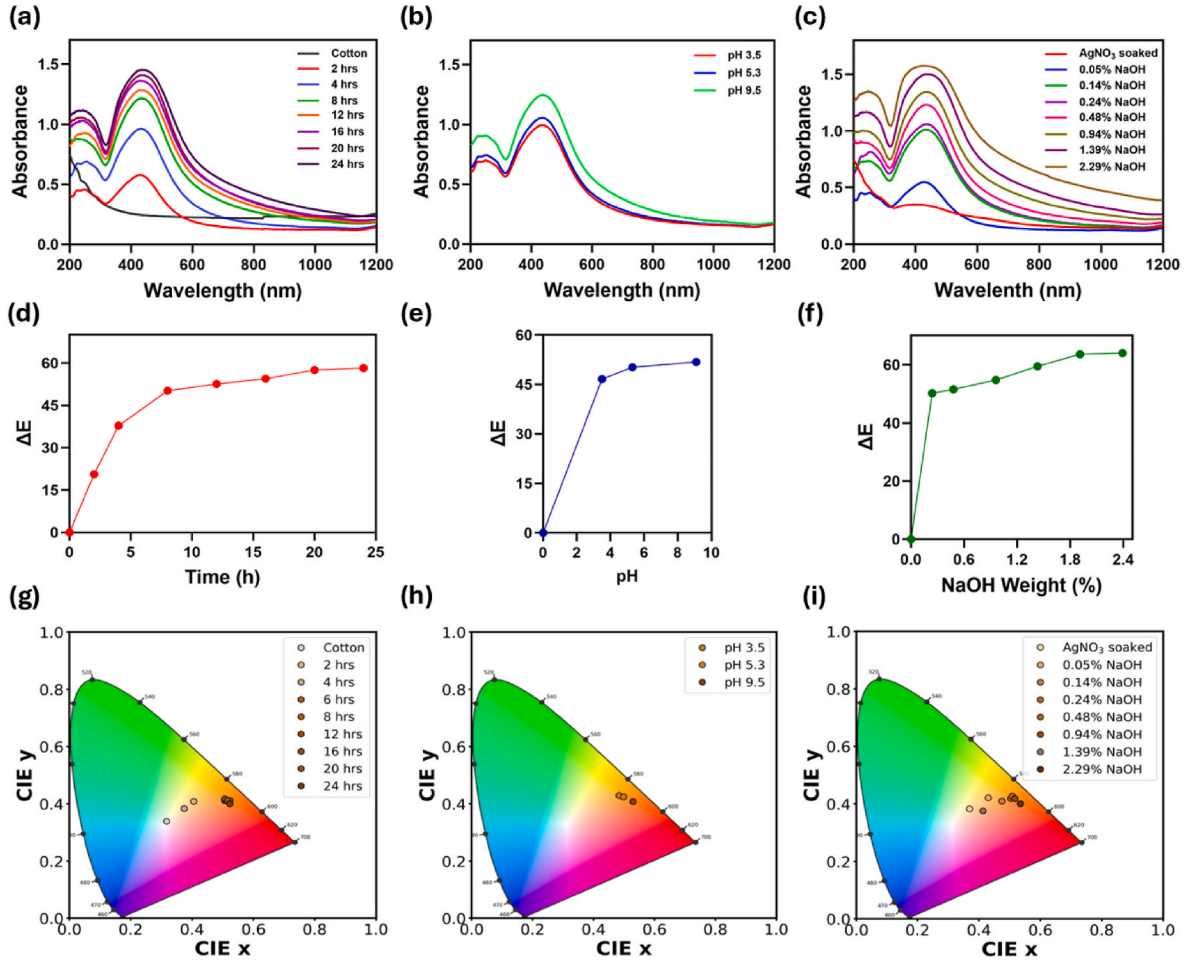

Fig. 2. UV-vis and colorimetric characterizations of various cotton fabrics, (a)-(c) UV-vis spectroscopy of cotton and NanoAgCot fabrics with respect to reaction time (a), initial soaking pH (b) and NaOH w/v% (c), (d)-(f) Δ E changes with respect to time (d), initial soaking pH (e) and NaOH w/v% (f), (g)-(i) CIE 1931 chromaticity graph depicting the color of the fabrics with respect to time (g), initial soaking pH (h) and NaOH w/v% (i).

3.2. UV-vis spectra and colorimetric characterization of the NanoAgCot fabric

Fig. 2 presents the UV–vis spectra of various cotton fabrics subjected to different treatments, highlighting the kinetics and reaction conditions governing AgNP formation. As expected, pristine cotton showed no distinct plasmonic features, consistent with the absence of Ag nanoparticles on the fabric (Fig. 2a). After soaking in $AgNO_3$ for 1 h at pH 5.3 and reacting with 0.24% (w/v) NaOH, the resulting NanoAgCot fabric displayed a characteristic surface plasmon resonance (SPR) band at 435 nm (Nam and Condon, 2014; Pranto et al., 2025). The peaks are redshifted with increasing reaction time from 2 to 24 h, which indicates an increase in nanoparticle size (Amirjani et al., 2020). The steady rise in SPR peak absorbance indicates progressive and uniform nanoparticle formation, reflecting the time-dependent growth of AgNPs within the microfibrillar network. The influence of initial soaking pH on nanoparticle formation was also investigated (Fig. 2b). Upon dissolution, $AgNO_3$ exhibited an inherent pH of 5.3, which was subsequently adjusted to 3.5 and 9.5 using HCl and NaOH, respectively. After reactions, NanoAgCot cotton samples demonstrated progressively increasing SPR peak absorbance with increasing pH. At pH 9.5, the enhanced SPR response is attributed to partial NaOH pretreatment during pH adjustment, which induces temporary fiber swelling and generates additional cellulose alkoxide sites, thereby promoting Ag^+ binding and reduction. In contrast, acidic conditions (pH 3.5) diminish the reducing capacity of cellulose by the protonation of the cellulose alcohols ($R\text{-}OH_2^+$) which inducing coulombic expansion at the molecular level and electrostatic repulsion of Ag^+. Consequently, nanoparticle formation was limited. Furthermore, the role of NaOH concentration was systematically examined (Fig. 2c). The NanoAgCot fabric treated with specific NaOH w/v% is denoted as $NanoAgCot_n$, where n is the nanoparticle concentration. Cotton fabric treated with 0.1 w/v% $AgNO_3$ without NaOH treatment displayed no significant SPR peak as shown in Fig. 2c. However, compared to the spectra of pristine cotton (Fig. 1a), the spectra of $AgNO_3$-soaked cotton showed a small curvature around 435 nm, probably due to absorption of Ag^+ ions. With increasing NaOH concentration while keeping the reaction time (8 h) and initial soaking pH (5.3) constant, the SPR absorbance rose sharply. As shown in Fig. S3, the bulk solution pH after 8 h of reaction with NaOH in the presence of cotton fabric increased exponentially with increasing NaOH concentration, plateauing beyond 2.5% (w/v). The corresponding SPR peak absorbance of the fabrics followed the same trend (Fig. S3). These results confirm that NaOH facilitates nucleation by elevating pH and activating additional sites. Beyond the plateau, nanoparticle growth occurs within these sites, leading to increased particle size and gradual agglomeration over time (as displayed in the SEM images described in section 3.4). The highest SPR peak absorbance (1.60 ± 0.05) was recorded for $NanoAgCot_{2.29}$ fabric as shown in Fig. 2c, very close to the plateaued concentration (2.5%) as observed in Fig. S3. At higher concentrations, UV–vis spectra of NanoAgCot fabrics exhibited plasmon band broadening and diminished peak (Figs. S3 and S4a), which indicates nanoparticle aggregation on the fabric. For example, NanoAgCot fabrics treated with 2.72% and 3.14% NaOH exhibited broad SPR peaks (Fig. S4a), with absorbance peaks at 360 and 516 nm for $NanoAgCot_{2.87}$ fabric, and at 350 and 500 nm with decreased intensity for the $NanoAgCot_{3.14}$ fabric. Therefore, the SPR peak at 435 nm was diminished. Similarly, $NanoAgCot_{3.14}$ fabric after 24 h of reaction exhibited reduced intensity with a broad peak (Fig. S4a). This was further supported by uneven coloration in $NanoAgCot_{3.14}$ fabric as shown in Fig. S4b. In contrast, $NanoAgCot_{0.5}$ exhibited a consistent SPR peak at 435 nm even after 48 h of reaction, attributable to the lower NaOH concentration (Fig. S4a). This observation further underscores the critical role of NaOH concentration in nanoparticle formation and highlights the potential for optimizing process parameters considering reaction time and NaOH concentration to enhance synthesis efficiency.

The sequence of reagent addition was found to be critical. When cotton was soaked in 1.39% (w/v) NaOH for 1 h prior to reaction with 0.1% (w/v) $AgNO_3$ for 8 h, broad and diminished SPR peak absorbance were observed in UV-vis spectra, as shown in Fig. S5, indicative of uncontrolled nucleation and aggregation of formed NPs. In contrast, presoaking with 0.1% (w/v) $AgNO_3$ followed by reaction with 1.39% (w/v) NaOH for 8 h resulted in a sharp SPR absorbance peak, indicating more controlled particle growth. Therefore, introducing $AgNO_3$ first, followed by NaOH, slowed the reduction rate and enabled control over nucleation site formation. Thus, this process promotes homogeneous nanoparticle distribution within a certain time frame and NaOH concentration. Mechanical agitation is also essential for achieving uniform nanoparticle distribution. NanoAgCot fabrics prepared under identical conditions (0.1% w/v $AgNO_3$, 1.39% w/v NaOH, initial pH 5.3, 8 h) showed distinct coloration depending on vortexing. $NanoAgCot_{1.39}$ fabric without any vortexing/shaking exhibited non-uniform coloration after synthesis, indicating uneven AgNP dispersion (Fig. S6). In contrast, the fabric subjected to continuous vortexing during synthesis displayed consistent and uniform coloration (Fig. S6), which reflects homogeneous nanoparticle deposition. Hence, continuous vortexing ensured effective diffusion of Ag^+ and OH^- ions, promoted homogeneous nucleation throughout the fiber, and suppressed uncontrolled nanoparticle aggregation, yielding more uniform particle deposition.

Colorimetric analysis of various NanoAgCot further corroborated these findings. Fig. 2d–f shows that ΔE values increased rapidly at early stages of reaction time, initial pH, and NaOH concentration before reaching a plateau, consistent with saturation of nanoparticle incorporation. The visible color evolution of the fabric under these conditions was mapped in CIE 1931 chromaticity space (Fig. 2g–i), where progressive shifts in chromaticity coordinates from light brown to dark brown color corresponded directly to nanoparticle loading. These optical transitions provide a rapid, non-destructive indicator of nanoparticle formation and distribution, in line with the UV–Vis results.

3.3. Optimization of the fabrication parameters

The fabrication parameters were further analyzed and optimized for effective nanoparticle formation. It was reported that UV–vis SPR peak absorbance correlates with nanoparticle concentration (Hillyer et al., 2022). To establish this quantitative relationship, silver content in various NanoAgCot fabrics was measured using Graphite Furnace Atomic Absorption Spectroscopy (GFAAS) and plotted against their corresponding SPR peak absorbance (Fig. 3a). The analysis revealed a clear exponential dependence of SPR peak absorbance on silver concentration in the fabric. The maximum nanoparticle loading was 22, 888 ± 2967 mg/kg for $NanoAgCot_{2.29}$ fabric. Beyond 1.62, the SPR peak absorbance decreased. This graph was later used to determine the amount of Ag present in fabrics after the laundering tests within the SPR peak absorbance range (0.5500-1.6200) and to compare these concentrations with those determined directly by GFAAS.

To optimize synthesis conditions for maximal nanoparticle formation with minimal particle aggregation based on SPR peak absorbance, Sequential Least Squares Quadratic Programming (SLSQP) was employed. At initial soaking pH 5.3, the model explored NaOH concentrations (0.05–3.15% w/v) and reaction times (2–20 h), yielding a SPR peak absorbance ranging from 0.5505 to 1.6200. Therefore, the constraints for the model were set as $0.05 \leq$ NaOH concentration $\leq 3.15\%$, 2 h $\leq$ reaction time ≤ 20 h, and $0.5 \leq$ SPR peak absorbance ≤ 1.62. Starting from an initial condition of 1.55% NaOH and 12 h for iterations, the optimum was identified at 1.91% NaOH and 8.65 h, corresponding to a predicted absorbance of 1.611. Fig. 3b presents a contour plot illustrating the relationship between SPR peak absorbance, NaOH concentration, and reaction time, with the predicted optimal point. The optimal condition reflects a mechanistic balance with sufficient silver ion reduction without triggering aggregation of nanoparticles. As shown in Fig. 3b, a distinct triangular bright region on the contour plot, representing high absorbance, emerges in the mid-range of

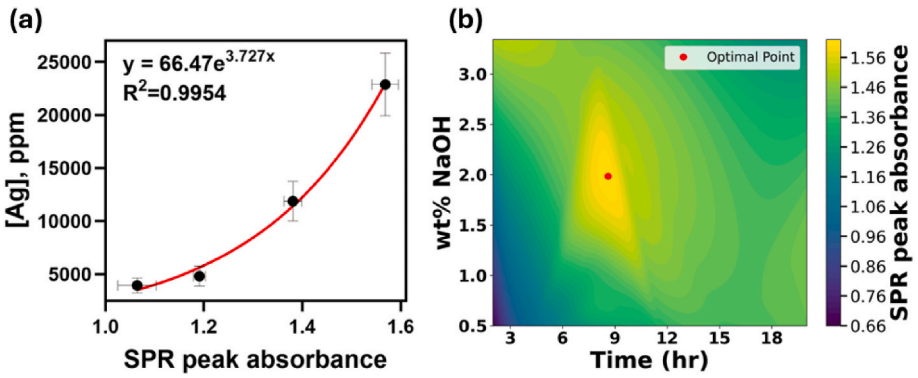

Fig. 3. Ag distribution and optimization, (a) Concentration of Ag with respect to SPR peak absorbance, (b) Optimization of NaOH w/v% and reaction time (h) for maximum SPR peak absorbance at fixed initial pH.

NaOH concentrations. Initially, SPR absorbance increases with reaction time and NaOH concentration driven by homogeneous nanoparticle formation. As NaOH concentration increases further, the high-absorbance region narrows and forms a triangular contour which indicates rapid growth and aggregation.

The statistical significance of the model was tabulated in Table S2. The model provided an excellent fit to the experimental data (R^2 = 0.8325, RMSE = 0.1402) and was statistically significant with $p = 2.32 \times 10^{-5}$, confirming that the selected variables adequately explain the observed variation in UV–vis absorbance. Among the factors, NaOH concentration (b_1 = 0.705, p = 00014) had the most dominant effect, followed by reaction time (b_2 = 0.053, p = 0.0022). The interaction term (b_{12} = −0.014, p = 0.0008) was highly significant and negative, indicating prolonged reaction time at high concentration led to a decrease in SPR peak absorbance. Both quadratic terms were negative and significant (p = 0.0083 and 0.0061, respectively). This observation supports the presence of non-linear curvature in the response surface and suggests diminishing returns at higher

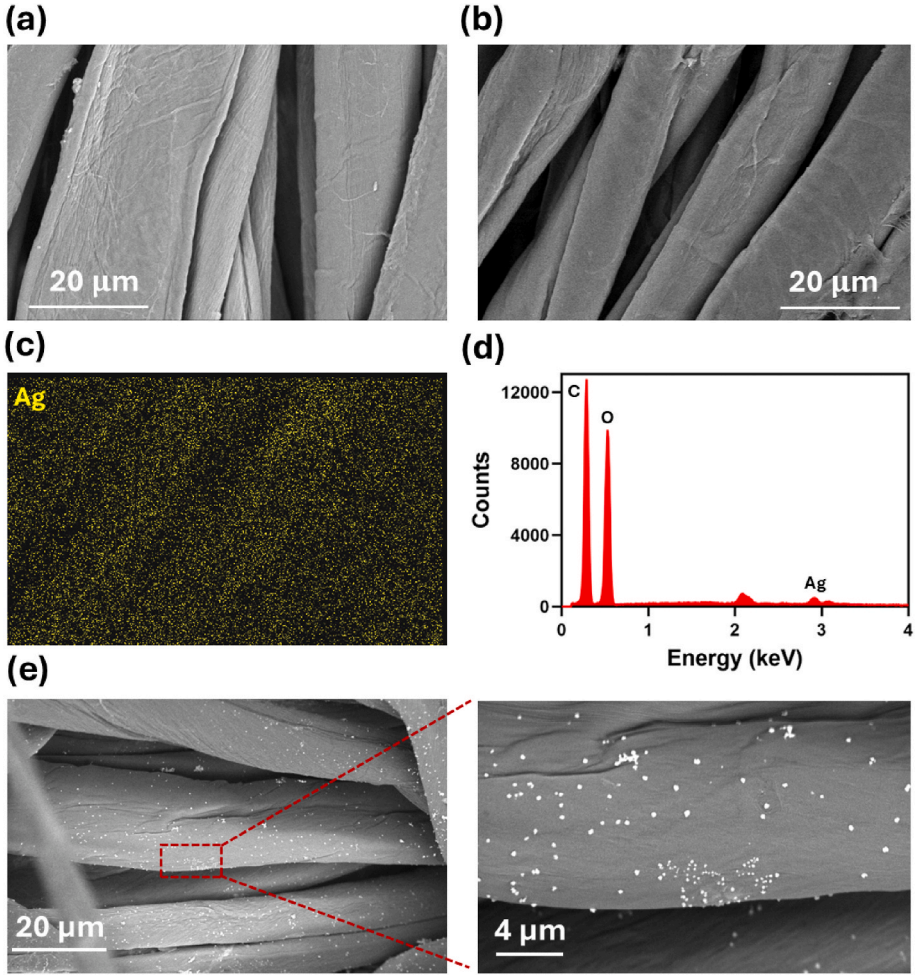

Fig. 4. Surface characterization of various NanoAgCot fabrics. (a–b) SEM micrographs of pristine cotton (a) and $NanoAgCot_{1.39}$ Fabric (b); (c) SEM–EDS elemental mapping showing silver distribution across the cotton matrix; (d) SEM–EDS spectrum confirming elemental composition of $NanoAgCot_{1.39}$ Fabric; (e) SEM image of $NanoAgCot_{1.96}$ Fabric, highlighting silver nanoparticles on fiber surface.

concentrations and longer times, due to nanoparticle agglomeration. Together, these findings highlight that optimal nanoparticle incorporation requires balancing concentration and reaction time, as excessive values of both variables lead to reduced efficiency.

3.4. Morphological analysis of NanoAgCot by SEM and TEM

Fig. 4 presents the morphological characterization of silver nanoparticles embedded on the surface of the NanoAgCot fiber through SEM analysis. As shown in Fig. 4a, pristine cotton exhibited a smooth fiber surface. Additionally, SEM-EDS elemental spectra of the fabric showed no Ag signal (Fig. S7). On the contrary, NanoAgCot$_{1.39}$ (Fig. 4b) fabric also did not show any visible nanoparticles in higher magnification. However, SEM-EDS elemental mapping revealed a uniform distribution of AgNPs along the fiber structure (Fig. 4c). Together, both images confirm no agglomeration of nanoparticles on the fiber surface. The presence of Ag was further confirmed by distinct Ag peaks in the SEM-EDS spectra (Fig. 4d). Quantitative analysis of NanoAgCot fabric indicated that surface and near-surface silver content ranged from 4.3 to 12.3 wt%, depending on the synthesis conditions.

To further elucidate nanoparticle morphology, a NanoAgCot$_{1.96}$ fabric sample was examined at higher magnification (Fig. 4e). The images revealed larger spherical nanoparticles resulting from treatment with elevated NaOH concentrations (1.96 w/v%). The nanoparticles were uniformly decorated on the fiber surface without significant aggregation. This morphology is consistent with the SPR absorption profiles in Fig. 2c, where the sharp peak was observed in fabrics treated up to 2.29% w/v NaOH concentration, indicating homogeneous distribution of nanoparticles on the fiber surface. Further increase in NaOH concentration to 2.72% (w/v) resulted in aggregation of the nanoparticle on the surface of NanoAgCot$_{2.72}$ fabric, as displayed in the SEM image in Fig. S8. This phenomenon is also consistent with the broad SPR peak absorbance observed in NanoAgCot fabrics treated with NaOH concentration greater than 2.29% w/v, as described in Fig. S3. Combinedly, the SEM–EDS results corroborate the spectroscopic and optimization analyses.

Beyond surface deposition, silver nanoparticles were also incorporated within the interior of cotton fibers, as demonstrated in Fig. 5. The cross-sectional SEM image in Fig. 5a of NanoAgCot$_{1.39}$ fiber clearly revealed numerous bright spots distributed across the fiber cross-section, indicative of silver-rich domains embedded within the cellulosic matrix. This observation confirms that Ag^{+} ions diffused deeply during the soaking step and subsequently underwent in-situ reduction throughout the fiber rather than being confined to the outer surface. Elemental confirmation was provided by SEM–EDS (Fig. 5b), which displayed distinct silver peaks in cross-sectional scans. The quantified Ag content ranged from 0.56 to 1.2 wt%, lower than surface concentration but significant enough to validate intrafibrillar nanoparticle incorporation. Transmission electron microscope (TEM) analysis further resolved the nanoscale morphology of these interfibrous nanoparticles. As shown in Fig. 5c, spherical nanoparticles were homogenously distributed across the fiber cross-section in NanoAgCot$_{1.39}$ fabric. Image analysis of TEM images of the nanoparticles using ImageJ (Fig. 5d) yielded an average diameter of 14.74 ± 6.61 nm. The small sizes of the nanoparticles are favorable for efficient antibacterial properties because they show faster release of Ag^{+} as reported by literature (Carlson et al., 2008; Dobias and Bernier-Latmani, 2013). Taken together, these findings demonstrate that the fabrication process yields hierarchical nanoparticle incorporation where AgNPs are anchored both on the fiber surface and within the bulk structure. Such dual localization enhances functional durability and provides a more robust interaction between nanoparticles and the cotton matrix.

3.5. XRD and XPS of NanoAgCot fabric

XRD analysis further confirms the reductive role of cotton fiber in AgNP formation. As shown in Fig. 6a, the precipitate from the reaction between 0.1% w/v $AgNO_3$ and 1.39% w/v NaOH in the absence of cotton fabric (red spectra) exhibited distinct diffraction peaks at 26.3°, 32.4°, 37.7°, 55.1°, 65.6°, and 69.2° corresponding to the (110), (202), (020), (220), (311) and (222) planes of Ag_2O (Elyamny et al., 2021; Rajabi et al., 2019; Zhan et al., 2019). These peaks are consistent with the formation of silver(I) oxide via the reaction:

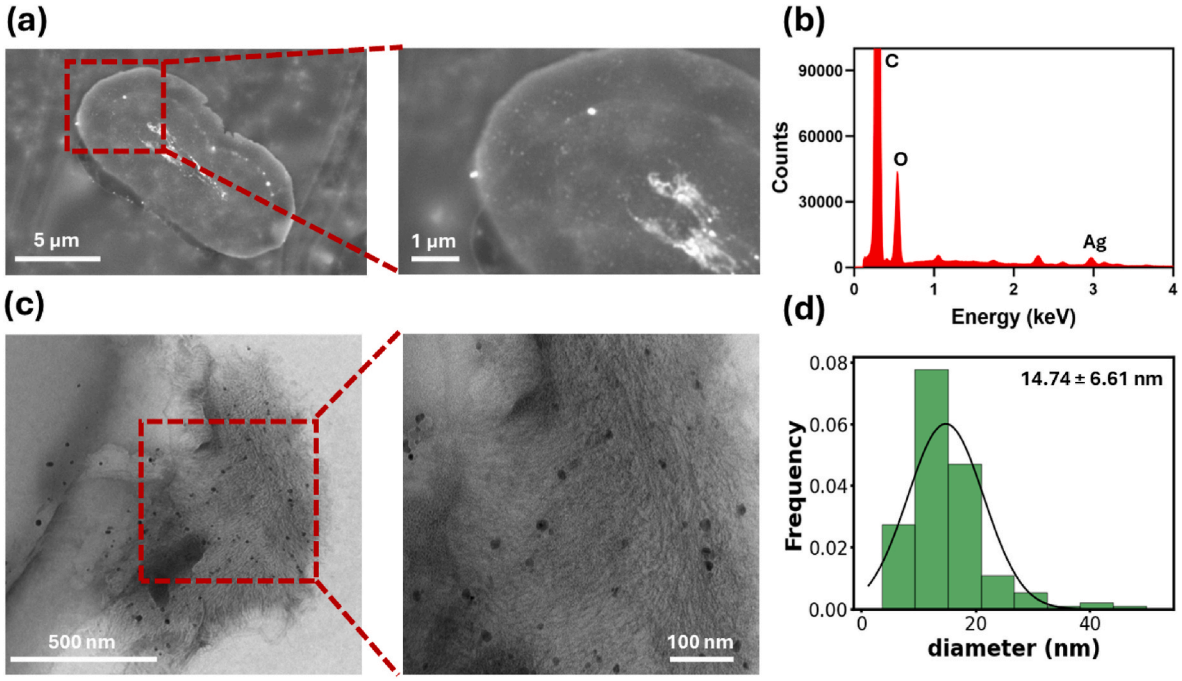

Fig. 5. Cross-sectional characterization of NanoAgCot fiber. (a) SEM micrograph of the fiber cross-section showing morphological features; (b) SEM–EDS elemental mapping confirming silver distribution across the fiber interior; (c) TEM image revealing intrafibrillar localization of AgNPs within the fiber matrix; (d) Size distribution of AgNPs across the cross-section, quantified via ImageJ analysis of TEM data.

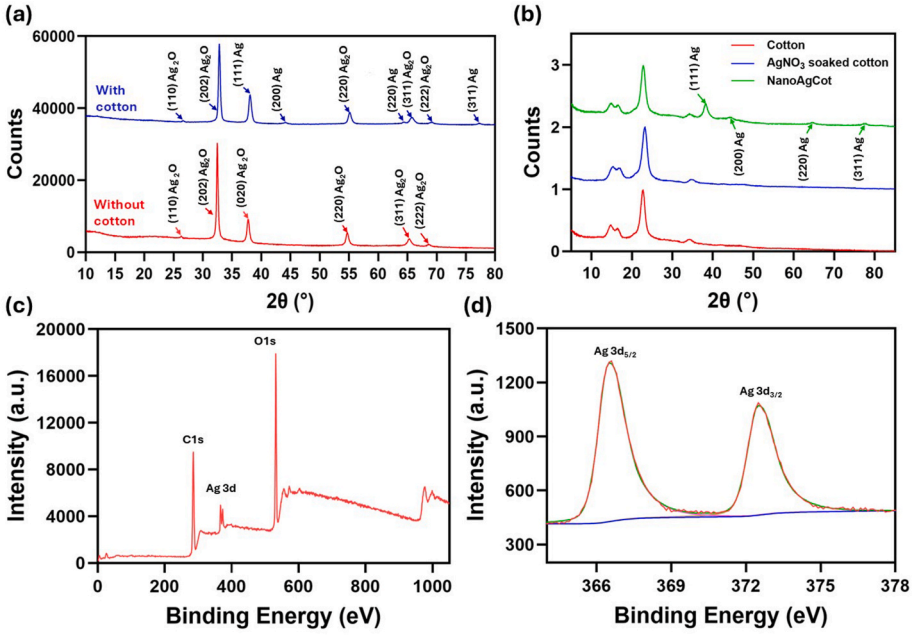

Fig. 6. XRD analysis of reaction precipitate and various cotton samples, (a) XRD spectra of reaction precipitates obtained after 8 h with and without NanoAgCot fabric, (b) XRD spectra of pristine cotton fabric, $AgNO_3$-soaked cotton fabric, and NanoAgCot fabric, (c)-(d) Survey spectra (c) and high-resolution spectra (d) of XPS of NanoAgCot fabric.

$$2\ AgNO_3 + 2\ NaOH \rightarrow Ag_2O + 2\ NaNO_3 + H_2O \qquad \text{Eq. (4)}$$

In contrast, when NanoAgCot fabric was present in the solution, additional peaks appeared (blue spectra) at 44.3°, 64.4°, and 77.3°, which correspond to the (200), (220), and (311) planes of face-centered cubic Ag, consistent with metallic AgNPs peaks reported in the literature (Nam and Condon, 2014; Pranto et al., 2025). There was a close overlap between the Ag and Ag_2O peaks at 38.1°, indicating the formation of a hybrid structure. Previous reports have attributed the diffraction peak near 38° to either metallic Ag or Ag_2O, thereby supporting the simultaneous presence of (111) Ag (38.1°) and (020) Ag_2O (38.0°) phases

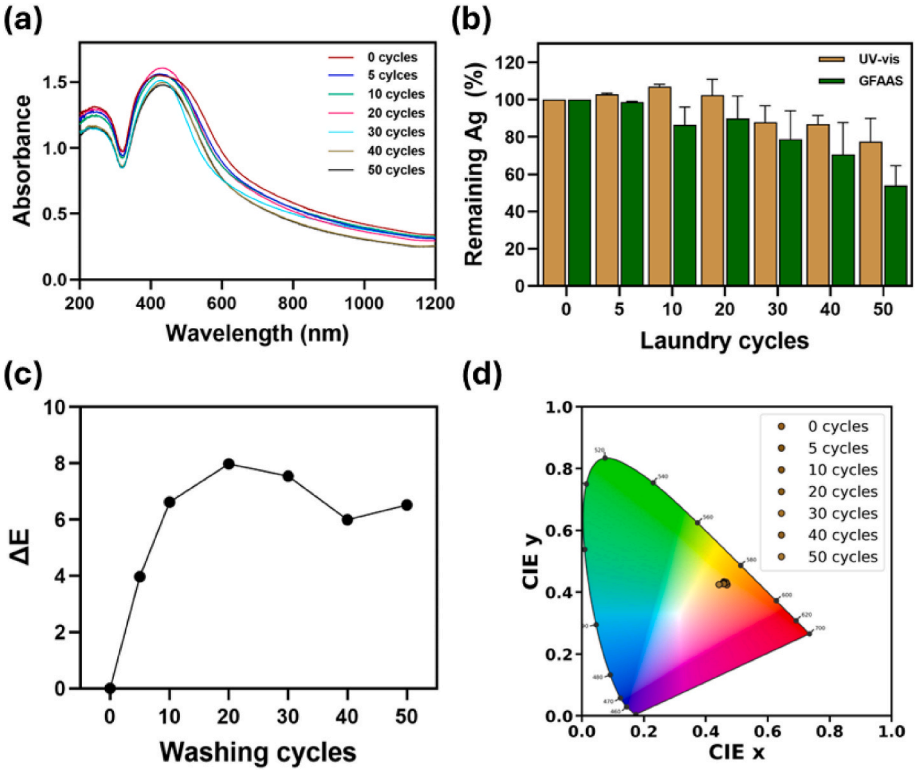

Fig. 7. Wash durability of NanoAgCot fabric, (a) UV–vis spectra of AgNP–cotton fabric after different wash cycles, (b) percentage of remaining silver determined by UV–vis and graphite furnace atomic absorption spectroscopy (GFAAS), (c) ΔE changes with respect to washing cycles, (d) CIE 1931 chromaticity graph depicting the color of the fabric at different wash cycles.

within the samples (Pranto et al., 2025; Ullah et al., 2020). Notably, there is a relatively low concentration of Ag NP in the precipitate with cotton. This emphasizes that Ag^0 is formed on/inside the fiber and mostly remains on the fiber. Fig. 6b compares the XRD spectra of pristine cotton, $AgNO_3$-soaked cotton, and NanoAgCot fabric. Characteristic cellulose Iβ peaks were observed in all fabric samples at $2\theta = 14.7°$, 16.6°, 22.7°, and 34.8°, corresponding to the (1–10), (110), (200), and (004) planes (Hillyer et al., 2022). Furthermore, the absence of the cellulose II (020) peak (Fig. 6b) in NanoAgCot fabric spectra confirmed that alkaline treatment did not alter the native crystalline structure. Importantly, the NanoAgCot fabric exhibited well-defined peaks corresponding to the (111), (200), (220), and (311) planes of metallic silver. On the contrary, there is no Ag_2O peak observed on the XRD of NanoAgCot fabric, demonstrating the reductive capacity of cotton.

Fig. 6b and c depict the XPS analysis of NanoAgCot fabric. The peaks for C1s and O1s of cotton cellulose were observed at 285 and 531 eV. High resolution spectra depict that two peaks at 367.54 eV and 373.54 eV were observed for Ag $3d_{5/2}$ and Ag $3d_{3/2}$, respectively, which is aligned with the literature for confirmation of Ag NP formation (Abdel-Fattah et al., 2015; Orfi et al., 2022).

3.6. Wash-durability of NanoAgCot fabric

Fig. 7 illustrates the wash durability of the $NanoAgCot_{1.39}$ fabric (18,586 ± 1206 mg/kg). As shown in Fig. 7a, the UV–vis spectra revealed an initial increase in the SPR peak absorbance for the first 20 cycles and a decrease afterwards. Silver concentration at different wash cycles was quantified using the calibration curve established in Fig. 3a and by GFAAS measurements (Fig. 7b). Ag content from UV–vis measurements revealed a gradual increase initially, reaching 110% after 20 washing cycles, followed by a decline to 80% after 50 cycles. The SPR peak absorbance reflects the concentration of AgNPs near the fabric surface (Nam et al., 2021). Therefore, the rise in absorbance can be attributed to the migration and reorganization of interfibrillar Ag^+ from the fiber interior to the surface through the dissolution and/or oxidation of Ag on the particle surface, likely induced by repeated mechanical impact from the steel balls during the laundering process. Silver ions diffuse toward the cotton fiber surface and adsorb onto pre-existing AgNPs (Nam et al., 2021). This surface adsorption alters particle morphology, resulting in a measurable shift in SPR peak absorbance. Beyond 20 cycles, the decrease in SPR intensity suggests progressive loss of nanoparticles up to 23%. However, it was previously reported that fabric containing interior nanoparticles predominantly releases Ag^+ during the laundering cycle, while fabric containing exterior nanoparticles released significantly higher amounts of particulate Ag, which poses a major environmental concern due to its potential to inhibit microbial activity in wastewater treatment systems and its long-term persistence in aquatic ecosystems (Nam et al., 2021). On the contrary, the GFAAS measurement displays a consistent decrease in Ag concentration. However, for the first 20 cycles, GFAAS indicates a slower decline in silver concentration followed by a rapid decline. After 50 washing cycles, the NanoAgCot fabric retained over 55% of its original silver content, which demonstrates markedly superior durability compared to prior reports (Nam et al., 2020). For instance, cotton fabric with silver nanoparticles fabricated via the pad-dry-cure method retained only 7% of the applied silver after just 20 cycles, highlighting the limitations of conventional surface treatment (Lee et al., 2003). Fig. 7c and d illustrate the ΔE values and corresponding fabric color changes across multiple washing cycles. The ΔE values progressively increase up to 20 cycles, suggesting surface particle reorganization and associated color variation. Beyond 20 cycles, a slight decrease followed by an increase at 50 cycles indicates nanoparticle loss from the surface. Notably, Fig. 7d shows that the fabric retains its brown hue, indicated by the clustered distribution of color, even after 50 washing cycles, visually confirming the presence of nanoparticles. XRD analysis of washed and unwashed fabrics confirmed the persistent presence of crystalline AgNPs, as shown in Fig. S9, further demonstrating the structural stability and durability of the nanoparticles within the cotton matrix even after 50 repeated laundering cycles.

3.7. Antibacterial property of NanoAgCot fabric

The antibacterial activity was investigated following the AATCC 100 test method against *Pantoea agglomerans* and *Pseudomonas aeruginosa* (both gram-negative bacteria), as well as *Bacillus subtilis* and *Staphylococcus aureus* (both gram-positive bacteria). As summarized in Table 1, the $NanoAgCot_{1.39}$ (18,586 ± 1206 mg/kg) fabric exhibited excellent antibacterial performance against all tested strains. Notably, NanoAgCot displayed complete inhibition against plant pathogens, *P. agglomerans* and *B. subtilis* as depicted in Fig. 8. It further exhibited 99.997% and >99.9997% reduction against the clinical pathogens,*P. aeruginosa* and *S. aureus*, respectively. This study revealed a promising opportunity for NanoAgCot fabric to design wearable antimicrobial textiles, such as coats and gloves for farm workers, to mitigate pathogen transmission from infected plants. The superior antibacterial effect can be attributed to the smaller size of the interfibrillar nanoparticle in NanoAgCot as reported in Fig. 5d. Herein, NanoAgCot fabric functions as a sustained reservoir for Ag^+ release. The liberated ions exert broad-spectrum antimicrobial activity through well-established mechanisms as follows: (i) induction of reactive oxygen species that trigger oxidative damage to DNA, proteins, and membrane lipids; (ii) disruption of membrane integrity via interactions with membrane proteins and phospholipids, causing loss of cellular contents; and (iii) inactivation of essential enzymes through strong binding to protein thiol groups, thereby impairing key metabolic pathways (Nam et al., 2025; Yamanaka et al., 2005). Together, these synergistic effects enable Ag^+ ions to efficiently inactivate diverse bacterial pathogens.

4. Conclusion

A streamlined one-pot room temperature synthesis method was developed for generating silver nanoparticles both inside and on the surface of cotton fibers, utilizing cotton cellulose as a reducing agent. Pre-soaking a white cotton fabric in an aqueous silver nitrate ($AgNO_3$) solution facilitated diffusion of Ag^+ ions into the fiber matrix. Subsequent alkali (NaOH) addition, coupled with continuous mechanical agitation, enabled controlled and homogeneous nanoparticle formation both on the surface and inside of the cotton fiber. During synthesis, cotton effectively reduced Ag^+ to metallic Ag^0, whereas in its absence, no Ag^0 formation was observed, thereby confirming the intrinsic reducing capacity of cellulose at room temperature without the need for additional chemical agents, external heat, or light which are extensively required in existing fabrication techniques. Utilizing sequential least squares programming (SLSQP), the optimized nanoparticle formation for maximum uniform nanoparticle loading was achieved at reaction time of 8.65 h and NaOH concentration of 1.91 w/v%. However, the process may generate nanoparticle agglomeration and uneven distribution of nanoparticles in longer reaction time and NaOH concentration. The resulting AgNPs exhibited an average size of 14.74 ± 6.61 nm, and the silver nanoparticle incorporated cotton (NanoAgCot) displayed a uniform light brown to dark brown color for a nanoparticle loading of 3,940 – 22,888 mg kg^{-1} which is significantly higher than other approaches considering the simplicity of the fabrication technique.

Table 1
Antibacterial efficacies of NanoAgCot against various pathogens.

Pathogen	Classification	% Inhibition
Pantoea agglomerans (BSDF19-4)	Gram-negative	100.00
Pseudomonas aeruginosa (ATCC 9027)	Gram-negative	99.997
Bacillus subtilis (BSDF49-1)	Gram-positive	100.00
Staphylococcus aureus (ATCC 6538)	Gram-positive	>99.9997

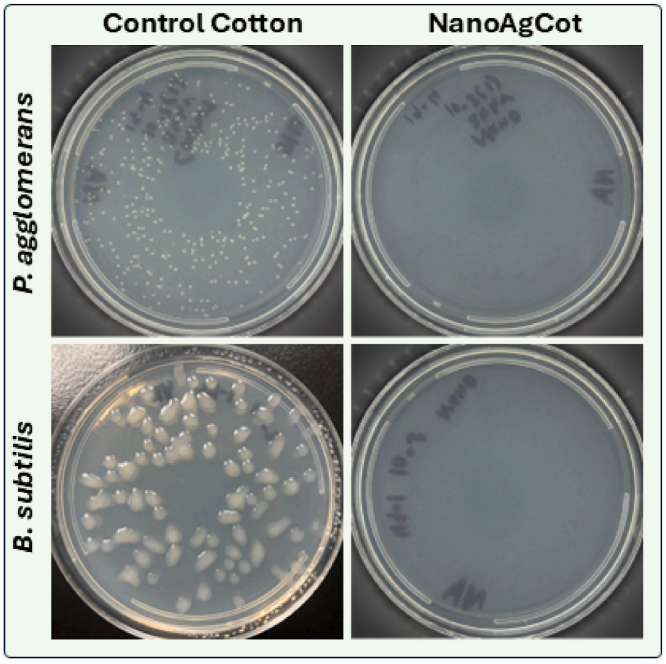

Fig. 8. Antibacterial efficacy of pristine cotton and NanoAgCot$_{1.39}$ fabrics against *Pantoea agglomerans* and *Bacillus subtilis* after 24 h of incubation.

Importantly, the nanoparticles were distributed both inside and on the surface of the cotton fiber was validated by SEM and TEM analysis resulting in improved laundering resistance and antimicrobial resistance.

The laundering durability test following the AATCC Test Method 61-2007 confirmed strong nanoparticle–fiber binding in NanoAgCot, where over 55% of total AgNPs were retained even after 50 laundering cycles due to interfibrillar nanoparticle distribution. The fabric also demonstrated excellent antibacterial efficacy, achieving complete inhibition of plant pathogens, *Pantoea agglomerans* and *Bacillus subtilis*, 99.997% inhibition of *Pseudomonas aeruginosa*, and >99.9997% inhibition of *Staphylococcus aureus*. These properties position the fabric as a promising candidate for protective wearables in healthcare and agricultural settings, as well as a versatile substrate for broader functional applications for packaging, and air filtration applications. Further studies are needed to investigate the cytotoxicity and antimicrobial efficiency of the fabric under different nanoparticle concentrations and contact times prepared by this technique.

Declaration of generative AI and AI-assisted technologies in the writing process

During the preparation of this work, the author used Microsoft Copilot in order to improve the readability and language of the manuscript. After using this tool/service, the author(s) reviewed and edited the content as needed and took full responsibility for the content of the published article.

CRediT authorship contribution statement

Md Nayeem Hasan Kashem: Conceptualization, Data curation, Formal analysis, Investigation, Methodology, Software, Validation, Visualization, Writing – original draft, Writing – review & editing. **Sunghyun Nam:** Conceptualization, Formal analysis, Funding acquisition, Investigation, Methodology, Project administration, Resources, Software, Supervision, Validation, Writing – original draft, Writing – review & editing. **Matthew B. Hillyer:** Project administration, Supervision, Writing – review & editing. **Faqrul Hassan:** Formal analysis, Validation, Writing – review & editing. **Sanjay Joshi:** Data curation, Investigation, Writing – original draft, Writing – review & editing. **Tia Zimmerman:** Data curation, Writing – review & editing. **Gillian Bruni:** Funding acquisition, Supervision, Writing – review & editing. **Holly King:** Data curation, Formal analysis, Writing – review & editing. **Doug Hinchliffe:** Supervision, Writing – review & editing. **David Fang:** Funding acquisition, Supervision, Writing – review & editing.

Declaration of competing interest

The authors declare no conflicts of interest.

Acknowledgment

This research was supported in part by an appointment to the Agricultural Research Service (ARS) Research Participation Program administered by the Oak Ridge Institute for Science and Education (ORISE) through an interagency agreement between the U.S. Department of Energy (DOE) and the U.S. Department of Agriculture (USDA). ORISE is managed by ORAU under DOE contract number DE-SC0014664. We thank the CRIS (6054-41000-108-000-D and 6054-30600-003-000D) and ARS Sustainable Sugar Beet Research Initiative for supporting this work. All opinions expressed in this paper are the author's and do not necessarily reflect the policies and views of USDA, DOE, or ORAU/ORISE.

Appendix A. Supplementary data

Supplementary data to this article can be found online at https://doi.org/10.1016/j.clet.2026.101178.

Data availability

Data will be available from corresponding authors upon reasonable request.

References

Abdel-Fattah, W., Eid, M., Hanafy, M., Hussein, M., Abd El-Moez, S.I., El-Hallouty, S., Mohamed, E., 2015. Verification of resistance to three mediated microbial strains and cancerous defense against MCF7 compared to HepG2 through microwave synthesized plant-mediated silver nanoparticle. Adv. Nat. Sci. Nanosci. Nanotechnol. 6 (3), 035002.

Ali, A., Haq, I.U., Akhtar, J., Sher, M., Ahmed, N., Zia, M., 2017. Synthesis of Ag-NPs impregnated cellulose composite material: its possible role in wound healing and photocatalysis. IET Nanobiotechnol. 11 (4), 477–484.

Amirjani, A., Firouzi, F., Haghshenas, D.F., 2020. Predicting the size of silver nanoparticles from their optical properties. Plasmonics 15 (4), 1077–1082.

Andersson, A.M., Weiss, N., Rainey, F., Salkinoja-Salonen, M., 1999. Dust-borne bacteria in animal sheds, schools and children's day care centres. J. Appl. Microbiol. 86 (4), 622–634.

Balamurugan, M., Saravanan, S., Soga, T., 2017. Coating of green-synthesized silver nanoparticles on cotton fabric. J. Coating Technol. Res. 14 (3), 735–745.

Boylston, E., Hinojosa, O., Hebert, J., 1991. A quick embedding method for light and electron microscopy of textile fibers. Biotech. Histochem. 66 (3), 122–124.

Cao, C., Wang, F., Lu, M., Zhou, Y., 2023. Facile preparation of cotton fabric modified with iron oxide nanoparticles with durable superhydrophobicity for oil/water separation. Mater. Chem. Phys. 307, 128127.

Carlson, C., Hussain, S.M., Schrand, A.M., Braydich-Stolle, L.K., Hess, K.L., Jones, R.L., Schlager, J.J., 2008. Unique cellular interaction of silver nanoparticles: size-dependent generation of reactive oxygen species. J. Phys. Chem. B 112 (43), 13608–13619.

Chen, C.-Y., Chiang, C.-L., 2008. Preparation of cotton fibers with antibacterial silver nanoparticles. Mater. Lett. 62 (21-22), 3607–3609.

Chou, W.L., Yu, D.G., Yang, M.C., 2005. The preparation and characterization of silver-loading cellulose acetate hollow fiber membrane for water treatment. Polym. Adv. Technol. 16 (8), 600–607.

Cotton Inc, C. I. Cotton Morphology and Chemistry. Cotton Incorporated. Retrieved 11/21 from https://www.cottoninc.com/quality-products/nonwovens/cotton-fiber-tech-guide/cotton-morphology-and-chemistry/.

Cruz, A.T., Cazacu, A.C., Allen, C.H., 2007. Pantoea agglomerans, a plant pathogen causing human disease. J. Clin. Microbiol. 45 (6), 1989–1992.

de man, rogosa and sharpe (MRS) agar, 2003. In: Corry, J.E.L., Curtis, G.D.W., Baird, R. M. (Eds.), Progress in Industrial Microbiology, 37. Elsevier, pp. 511–513. https://doi.org/10.1016/S0079-6352(03)80066-8.
Dobias, J., Bernier-Latmani, R., 2013. Silver release from silver nanoparticles in natural waters. Environ. Sci. Technol. 47 (9), 4140–4146.
Dolez, P.I., 2021. Energy harvesting materials and structures for smart textile applications: recent progress and path forward. Sensors 21 (18), 6297.
Dubas, S.T., Kumlangdudsana, P., Potiyaraj, P., 2006. Layer-by-layer deposition of antimicrobial silver nanoparticles on textile fibers. Colloids Surf. A Physicochem. Eng. Asp. 289 (1-3), 105–109.
Dutkiewicz, J., Mackiewicz, B., Lemieszek, M.K., Golec, M., Milanowski, J., 2016. Pantoea agglomerans: a mysterious bacterium of evil and good. Part III. Deleterious effects: infections of humans, animals and plants. Ann. Agric. Environ. Med. 23 (2).
Ekunde, R.A., Sutar, R.S., Ingole, S.S., Jundle, A.R., Gaikwad, P.P., Saji, V.S., Liu, S., Bhosale, A.K., Latthe, S.S., 2025. Fluorine-free and breathable self-cleaning superhydrophobic CS/PDMS/PLA coatings on wearable cotton fabric with light-induced self-sterilization. Prog. Org. Coating 208, 109514.
El-Seedi, H.R., El-Shabasy, R.M., Khalifa, S.A., Saeed, A., Shah, A., Shah, R., Iftikhar, F.J., Abdel-Daim, M.M., Omri, A., Hajrahand, N.H., 2019. Metal nanoparticles fabricated by green chemistry using natural extracts: biosynthesis, mechanisms, and applications. RSC Adv. 9 (42), 24539–24559.
Elyamny, S., Eltarahony, M., Abu-Serie, M., Nabil, M.M., Kashyout, A.E.-H.B., 2021. One-pot fabrication of Ag@ Ag2O core–shell nanostructures for biosafe antimicrobial and antibiofilm applications. Sci. Rep. 11 (1), 22543.
Emam, H.E., Ahmed, H.B., 2016. Polysaccharides templates for assembly of nanosilver. Carbohydr. Polym. 135, 300–307.
Emam, H.E., El-Bisi, M., 2014. Merely Ag nanoparticles using different cellulose fibers as removable reductant. Cellulose 21 (6), 4219–4230.
Fazli, M., Bjarnsholt, T., Kirketerp-Møller, K., Jørgensen, B., Andersen, A.S., Krogfelt, K. A., Givskov, M., Tolker-Nielsen, T., 2009. Nonrandom distribution of Pseudomonas aeruginosa and Staphylococcus aureus in chronic wounds. J. Clin. Microbiol. 47 (12), 4084–4089.
Fu, W., Yu, B., Ji, D., Zhou, Z., Li, X., Wang, R., Lu, W., Sun, Y., Dai, Y., 2024. Intelligent fibers and textiles for wearable biosensors. Respons. Mater. 2 (4), e20240018.
Guodong, Y., Xu, Z., Qiuju, L., Yuanqing, W., Zhenzi, J., Fangming, J., 2012. Direct and Highly Efficient Reduction of NiO into Ni with Cellulose Under Hydrothermal Conditions.
Haynes, W., Wickerham, L., Hesseltine, C., 1955. Maintenance of cultures of industrially important microorganisms. Appl. Microbiol. 3 (6), 361–368.
Heymann, E., Rabinov, G., 1941. The acid nature of cellulose. I. Equilibria between cellulose and salts. J. Phys. Chem. 45 (8), 1152–1166.
Hillyer, M.B., Jordan, J.H., Ernst, N.E., Nam, S., Easson, M.W., 2024. Cu2O/CuO nanoparticle-cotton fiber biocomposite catalyst: Self-improvement through morphological changes during methyl Orange degradation. Langmuir 40 (52), 27174–27182.
Hillyer, M.B., Nam, S., Condon, B.D., 2022. Intrafibrillar dispersion of cuprous oxide (Cu2O) nanoflowers within cotton cellulose fabrics for permanent antibacterial, antifungal and antiviral activity. Molecules 27 (22), 7706.
Islam, J.M., Mondal, M.I.H., Das, S.C., 2021. The life and durability issues of natural textiles and clothing. In: Fundamentals of Natural Fibres and Textiles. Elsevier, pp. 657–690.
Kashem, M.N.H., Nam, S., Hillyer, M.B., Hassan, F., Li, W., Fang, D.D., 2025. Nanoengineered hydrophobic cotton fabric via surface functionalization of cuprous oxide (Cu2O) nanoflowers. Appl. Surf. Sci. 711, 163980.
Kumar, A., Mishra, B., Tripathi, B.P., 2020. Polydopamine assisted synthesis of ultrafine silver nanoparticles for heterogeneous catalysis and water remediation. Nano-Struct. Nano-Objects 23, 100489.
Lee, H.J., Yeo, S.Y., Jeong, S.H., 2003. Antibacterial effect of nanosized silver colloidal solution on textile fabrics. J. Mater. Sci. 38 (10), 2199–2204.
Li, H., Yu, J., Zeng, Z., Liu, C., Zhang, Y., Xia, H., Guo, S., 2024. Clinical and pathological features of cerebrospinal meningitis caused by Pantoea agglomerans: a case report. BMC Infect. Dis. 24 (1), 1150.
Li, Q., Yao, G., Zeng, X., Jing, Z., Huo, Z., Jin, F., 2012. Facile and green production of Cu from CuO using cellulose under hydrothermal conditions. Ind. Eng. Chem. Res. 51 (7), 3129–3136.
Lim, S.-H., Hudson, S.M., 2004. Application of a fiber-reactive chitosan derivative to cotton fabric as an antimicrobial textile finish. Carbohydr. Polym. 56 (2), 227–234.
Mani, S., Nair, J., 2021. Pantoea infections in the neonatal intensive care unit. Cureus 13 (2).
Mardaneh, J., Pouresmaeil, O., 2024. Pantoea Agglomerans: an emerging pathogen in hospitals and foods, A narrative review. Rev. Clin. Med. 11 (2).
Meresht, H.K., Talesh, S.S.A., Mahdavi, R., 2025. Superhydrophobic/superoleophilic porous adsorbents for oil–water separation: a comprehensive review of materials, fabrication techniques, and performance assessments. Environ. Sci. Pollut. Control Ser. 1–35.
Mirtella, D., Fedeli, P., Scendoni, R., Cannovo, N., Cingolani, M., 2021. A case of nosocomial outbreak of Pantoea agglomerans related to parenteral nutrition procedures. Healthcare 9 (6).
Nam, S., Chavez, S.E., Hillyer, M.B., Condon, B.D., Shen, H., Sun, L., 2021a. Interior vs. exterior incorporation of silver nanoparticles in cotton fiber and washing durability. AATCC J. Res. 8 (6), 1–12.
Nam, S., Easson, M.W., Jordan, J.H., He, Z., Lima, I.M., Hillyer, M.B., Ernst, N.E., Fang, D., Islam, M.M., 2024. Repurposing cotton gin trash for cellulose Nanofibril–Silver hybrid and ultralight silver-infused aerogel. ACS Omega 9 (36), 38195–38204.
Nam, S., Hillyer, M.B., Condon, B.D., Lum, J.S., Richards, M.N., Zhang, Q., 2020. Silver nanoparticle-infused cotton fiber: durability and aqueous release of silver in laundry water. J. Agric. Food Chem. 68 (46), 13231–13240.
Nam, S., Olanya, O.M., Jordan, J.H., Uknalis, J., He, Z., Kashem, M.N.H., Fang, D., 2025. From cotton gin byproduct to nano-in-nano structured hybrid composite for effective pathogen control. Front. Nanotechnol. 7, 1567693.
Nam, S., Selling, G.W., Hillyer, M.B., Condon, B.D., Rahman, M.S., Chang, S., 2021b. Brown cotton fibers self-produce Ag nanoparticles for regenerating their antimicrobial surfaces. ACS Appl. Nano Mater. 4 (12), 13112–13122.
Nam, S., Condon, B.D., 2014. Internally dispersed synthesis of uniform silver nanoparticles via in situ reduction of [Ag (NH3) 2]+ along natural microfibrillar substructures of cotton fiber. Cellulose 21 (4), 2963–2972.
Nicolas, P., Mäder, U., Dervyn, E., Rochat, T., Leduc, A., Pigeonneau, N., Bidnenko, E., Marchadier, E., Hoebeke, M., Aymerich, S., 2012. Condition-dependent transcriptome reveals high-level regulatory architecture in Bacillus subtilis. Science 335 (6072), 1103–1106.
Orfi, H., Mekkaoui, A.A., Sündü, B., Laayati, M., Labyad, S.A., El Firdoussi, L., Metin, Ö., El Houssame, S., 2022. Ag, Co3O4, Ag–Co3O4, and Ag/Co3O4 nanoparticles decorated mesoporous natural phosphate: effect of metal synergy and preparation method on the catalytic reduction reaction. J. Inorg. Organomet. Polym. Mater. 32 (6), 2192–2208.
Pranto, M., Kabir, M., Haque, M., Hasan, M., Saha, J., Rahman, M., Islam, T., Das, S., 2025. Synthesis of silk fibroin and silver nanoparticles for enhanced functionality in cellulosic textiles. Sci. Rep. 15 (1), 38559.
Qi, L., Zhang, K., Qin, W., Hu, Y., 2020. Highly efficient flow-through catalytic reduction of methylene blue using silver nanoparticles functionalized cotton. Chem. Eng. J. 388, 124252.
Qi, Y., Terrell, E., Bruni, G.O., Yassin, Z., Kandel, S.L., 2025. Microbial isolates from north American sugar beet factory juices and biofilms. J. Sugar Beet Res. 62 (1).
Rajabi, A., Ghazali, M.J., Mahmoudi, E., Baghdadi, A.H., Mohammad, A.W., Mustafah, N. M., Ohnmar, H., Naicker, A.S., 2019. Synthesis, characterization, and antibacterial activity of Ag2O-loaded polyethylene terephthalate fabric via ultrasonic method. Nanomaterials 9 (3), 450.
Salama, A., Abouzeid, R., Owda, M., Cruz-Maya, I., Guarino, V., 2021. Cellulose–silver composites materials: preparation and applications. Biomolecules 11, 1684.
Saleh, F., Kheirandish, F., Azizi, H., Azizi, M., 2014. Molecular diagnosis and characterization of Bacillus subtilis isolated from burn wound in Iran. Res. Mol. Med. 2 (2), 40–44.
Salgado, P., Bustamante, L., Carmona, D.J., Melendrez, M.F., Rubilar, O., Salazar, C., Perez, A.J., Vidal, G., 2023. Green synthesis of Ag/Ag2O nanoparticles on cellulose paper and cotton fabric using Eucalyptus globulus leaf extracts: toward the clarification of formation mechanism. Surf. Interfaces 40, 102928.
Sengupta, M., Banerjee, S., Das, N.K., Guchhait, P., Misra, S., 2016. Early onset neonatal septicaemia caused by Pantoea agglomerans. J. Clin. Diagn. Res.: J. Clin. Diagn. Res. 10 (5), DD01.
Seth, M., Jana, S., 2022. Green synthesis of hierarchically structured Ag–Cu2O on cotton fabric with sustained antimicrobial activity and on-demand oil–water separation ability. Cellulose 29 (8), 4703–4724.
Shi, Y., Zhang, Z., Huang, Q., Lin, Y., Zheng, Z., 2023. Wearable sweat biosensors on textiles for health monitoring. J. Semiconduct. 44 (2), 021601.
Sivaranjana, P., Nagarajan, E., Rajini, N., Jawaid, M., Rajulu, A.V., 2017. Cellulose nanocomposite films with in situ generated silver nanoparticles using Cassia alata leaf extract as a reducing agent. Int. J. Biol. Macromol. 99, 223–232.
Österberg, M., Claesson, P.M., 2000. Interactions between cellulose surfaces: effect of solution pH. J. Adhes. Sci. Technol. 14 (5), 603–618.
Tang, B., Zhang, M., Hou, X., Li, J., Sun, L., Wang, X., 2012. Coloration of cotton fibers with anisotropic silver nanoparticles. Ind. Eng. Chem. Res. 51 (39), 12807–12813.
Thibodeaux, D.P., Evans, J.P., 1986. Cotton fiber maturity by image analysis. Textil. Res. J. 56 (2), 130–139.
Trizna, E.Y., Yarullina, M.N., Baidamshina, D.R., Mironova, A.V., Akhatova, F.S., Rozhina, E.V., Fakhrullin, R.F., Khabibrakhmanova, A.M., Kurbangalieva, A.R., Bogachev, M.I., 2020. Bidirectional alterations in antibiotics susceptibility in Staphylococcus aureus—Pseudomonas aeruginosa dual-species biofilm. Sci. Rep. 10 (1), 14849.
Tsague, F.L., Chimeni, D.Y., Assonfack, H.L., Abo, M.T., Cheumani, A.M.Y., Ndinteh, D. T., Ndikontar, M.K., 2024. Study of oxidation of cellulose by Fenton-type reactions using alkali metal salts as swelling agents. Cellulose 31 (11), 6643–6661.
Ullah, S., Khan, A.A., Jan, A., Aain, S.Q., Neto, E.P., Serge-Correales, Y.E., Parveen, R., Wender, H., Rodrigues-Filho, U.P., Ribeiro, S.J., 2020. Enhanced photoactivity of BiVO4/Ag/Ag2O Z-scheme photocatalyst for efficient environmental remediation under natural sunlight and low-cost LED illumination. Colloids Surf. A Physicochem. Eng. Asp. 600, 124946.
Vance, M.E., Kuiken, T., Vejerano, E.P., McGinnis, S.P., Hochella Jr, M.F., Rejeski, D., Hull, M.S., 2015. Nanotechnology in the real world: redeveloping the nanomaterial consumer products inventory. Beilstein J. Nanotechnol. 6 (1), 1769–1780.
Wakelyn, P.J., Bertoniere, N.R., French, A.D., Thibodeaux, D.P., Triplett, B.A., Rousselle, M.-A., Goynes Jr, W.R., Edwards, J.V., Hunter, L., McAlister, D.D., 2006. Cotton Fiber Chemistry and Technology. CRC Press.
Xiong, J., Lin, M.F., Wang, J., Gaw, S.L., Parida, K., Lee, P.S., 2017. Wearable all-fabric-based triboelectric generator for water energy harvesting. Adv. Energy Mater. 7 (21), 1701243.
Yamanaka, M., Hara, K., Kudo, J., 2005. Bactericidal actions of a silver ion solution on Escherichia coli, studied by energy-filtering transmission electron microscopy and proteomic analysis. Appl. Environ. Microbiol. 71 (11), 7589–7593.

Yazdanshenas, M.E., Shateri-Khalilabad, M., 2012. The effect of alkali pre-treatment on formation and adsorption of silver nanoparticles on cotton surface. Fibers Polym. 13 (9), 1170–1178.
Yazdanshenas, M.E., Shateri-Khalilabad, M., 2013. In situ synthesis of silver nanoparticles on alkali-treated cotton fabrics. J. Ind. Textil. 42 (4), 459–474.
Zhan, T., Ding, G., Cao, W., Li, J., She, X., Teng, H., 2019. Amperometric sensing of catechol by using a nanocomposite prepared from Ag/Ag2O nanoparticles and N, S-doped carbon quantum dots. Microchim. Acta 186 (11), 743.
Zhang, R., Wang, J., Xue, L., Kamran, M., Wang, Y., Wei, X., Zhao, G., Li, C., 2025. The impact of bacterial leaf blight disease (Pantoea agglomerans) on grain yield and nutritional quality of oat. Microorganisms 13 (1), 141.